

# Fundamentals of the Reaction-Diffusion Process in Model EUV Photoresists<sup>§</sup>

Kristopher A. Lavery\*<sup>a</sup>, Kwang-Woo Choi\*<sup>b</sup>, Bryan D. Vogt<sup>a</sup>, Vivek M. Prabhu\*<sup>a</sup>, Eric K. Lin<sup>a</sup>, Wen-li Wu<sup>a</sup>, Sushil K. Satija<sup>c</sup>, Michael J. Leeson<sup>d</sup>, Heidi B. Cao<sup>d</sup>, George Thompson<sup>b</sup>, Hai Deng<sup>b</sup>, David S. Fryer<sup>d</sup>

<sup>a</sup>Polymers Division, National Institute of Standards and Technology, Gaithersburg, MD

<sup>b</sup>Intel Corporation, Santa Clara, CA

<sup>c</sup>Center for Neutron Research, National Institute of Standards and Technology, Gaithersburg, MD

<sup>d</sup>Intel Corporation, Hillsboro, OR

## ABSTRACT

More demanding requirements are being made of photoresist materials for fabrication of nanostructures as the feature critical dimensions (CD) decrease. For extreme ultraviolet (EUV) resists, control of line width roughness (LWR) and high resist sensitivity are key requirements for their success. The observed LWR and CD values result from many factors in interdependent processing steps. One of these factors is the deprotection interface formed during the post-exposure bake (PEB) step. We use model EUV photoresist polymers to systematically address the influence of exposure-dose on the spatial evolution of the deprotection reaction at a model line edge for fixed PEB time using neutron reflectivity. The bilayer consists of an acid feeder layer containing photoacid generator (PAG) and a model photoresist polymer, poly(hydroxystyrene-co-*tert*-butylacrylate) with perdeuterated *t*-butyl protecting group. The deuterium labeling allows the protection profile to be measured with nanometer resolution. The evolution of two length scales that contribute to the compositional profile is discussed.

Keywords: Photolithography, chemically amplified photoresists, diffusion

## INTRODUCTION

Next-generation advances in semiconductor technologies rely on the continued development of lithographic processes towards the target of sub-50 nm structure fabrication. The chemical amplification process remains the predominant platform for photolithography<sup>1</sup>, however, reaction-diffusion processes occurring within the resist during the post-exposure bake (PEB) step<sup>2,4</sup> contribute to image blurring and line-width roughness (LWR)<sup>5</sup>. The desire to control LWR to levels below 2 nm ( $3\sigma$ ) necessitates an understanding of the reaction front propagation at the exposure line edge<sup>6,7</sup>. Material factors<sup>8,9</sup> related to the coupled acid diffusion and deprotection reaction chemistry<sup>10</sup> must be thoroughly understood to deconvolute the origins of LWR.

As critical dimensions are driven below 45 nm, extreme ultra-violet (EUV) lithography is a candidate for achieving this goal. Exposures at 13.4 nm, however, carry their own sets of challenges. For example, source limitations will tend to keep exposure doses low; likely below 10 mJ/cm<sup>2</sup>. In order to compensate for these low doses, large PAG loadings are expected<sup>11</sup>, pushing loading levels as high as 40 % by mass. Thinner photoresist films are anticipated<sup>12</sup> to accommodate transparency and etch resistance, as well as feature aspect ratio criteria. Much work on reaction-diffusion front fundamental analyses<sup>13-17</sup> has been performed on homopolymer-based resist systems. However, high sensitivity, copolymeric resists will certainly need to be utilized in EUV applications. In addition, additives, such as base

---

<sup>§</sup> Official contribution of the National Institute of Standards and Technology; not subject to copyright in the United States

\* klavery@nist.gov, kwang-woo.choi@intel.com, vprabhu@nist.gov

quencher<sup>18,19</sup>, will play a prominent role. The influence of all of these factors on latent image formation will have to be understood.

In this work we illustrate a means of systematically studying the reaction-diffusion front propagation in a model EUV resist polymer. We do this by making use of a polymer-polymer bilayer geometry which mimics a sharp exposure line edge<sup>20</sup>. This is accomplished by loading the bottom layer with PAG and using a resist copolymer as the top layer, in which the protecting side-group is deuterium labeled. Upon exposure and PEB, the photoacid diffuses from the acid-feeder layer into the resist copolymer, initiating the catalytic deprotection reaction. This leads to a compositional broadening at the polymer-polymer interface. The form and deprotection extent at the buried interface is directly measured with sub-nm resolution using neutron reflectivity. The front propagation was studied as a function of exposure dose, or photogenerated acid concentration, at two temperatures. Correlations between the form of the latent image and copolymer chemistry are provided.

## EXPERIMENTAL METHODOLOGY<sup>#</sup>

### 1. Materials

The photoresist used was poly(hydroxystyrene-*co*-D9-*tert*-butyl acrylate) (P(HOST-*co*-tBA)) (number average molecular weight (Mn) = 11,700 g/mol, polydispersity index (PDI) = 1.75, 50/50 mole fraction, DuPont Electronic Materials), in which the 9 hydrogens of the *tert*-butyl protecting group were replaced with deuterium. The acid feeder layer consisted of poly(hydroxyladamantyl methacrylate) (PHAdMA) (Mn = 10,500 g/mol, PDI = 1.12, DuPont Electronic Materials). The photoacid generator used was triphenylsulfonium perfluorobutane sulfonate (TPS-PFBS) (Sigma-Aldrich). The PHAdMA/TPS-PFBS solution in *n*-butanol was spincoated onto silicon wafers (76 mm diameter, 700  $\mu\text{m}$  thick, Virginia Semiconductor, Inc.) that were cleaned by 5 min exposure to oxygen plasma, followed by removal of native oxide layer by immersion into a solution of (10  $\pm$  2) % volume fraction HF and (5  $\pm$  2) % volume fraction  $\text{NH}_3\text{F}$  in ultra pure water. An oxide layer was re-grown in a UV/Ozone chamber for (120  $\pm$  1) s. The acid feeder layer was post-apply baked (PAB) for 1 min at 130  $^\circ\text{C}$ . The resist polymer was spun coat from a solution in propylene glycol methyl ether acetate (PGMEA) on top of the acid feeder layer, followed by an additional PAB for 1 min at 130  $^\circ\text{C}$ . The different bilayer samples were then exposed to 248 nm broad-band radiation for a series of different times resulting in doses ranging from (0 to 20)  $\text{mJ}/\text{cm}^2$  followed by a post-exposure bake (PEB) at 90  $^\circ\text{C}$  or 130  $^\circ\text{C}$  for 30 s.

### 2. Methods

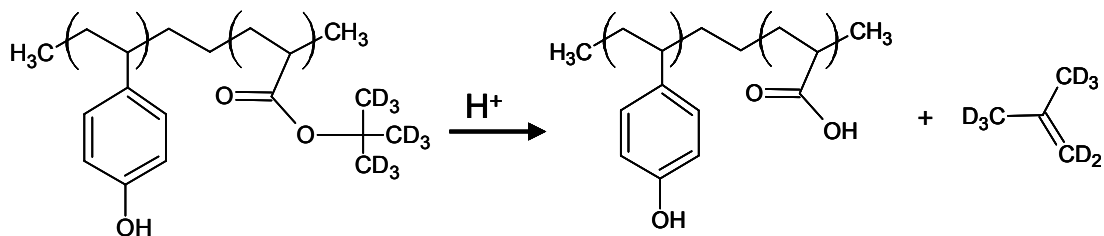
Neutron reflectivity (NR) experiments were completed at the NIST Center for Neutron Research (NCNR) on the NG-7 cold neutron reflectometer. The instrumental configuration included a neutron wavelength ( $\lambda$ ) of 4.768  $\text{\AA}$  with a wavelength spread ( $\Delta\lambda/\lambda$ ) = 0.025. The large neutron scattering length density difference between P(HOST-*co*-tBA) and PHAdMA provides sufficient contrast to resolve the bilayer structure and allow interfacial characterization. The scattering length density of the P(HOST-*co*-tBA) layer is significantly reduced upon deprotection, with the loss of deuterated *tert*-butyl groups allowing the direct observation of the reaction front at the interface. With the Parratt algorithm, the calculated reflectivity from the trial  $Q_c^2$  profile is fit to the experimental data using a Levenberg-Marquardt<sup>21</sup> non-linear least squares method with adjustable thickness, scattering length densities, and interfacial width of the unknown layers with least-squares statistic ( $\chi^2$ ). Uncertainties are calculated as the estimated standard deviation from the mean. In the case where the limits are smaller than the plotted symbols, the limits are left out for clarity.

The simplified deprotection chemistry is shown in Scheme 1. The deuterated isobutylene reaction product is volatile and leaves the film. The integrated deprotection level is monitored using Fourier transform infrared spectroscopy (FT-IR) in transmission normal to the bilayer sample. N-type, phosphorus-doped, <100> orientated silicon wafers were used with a resistance of (1 to 50) ohm cm in order to minimize the absorption of the infrared beam. FT-IR

---

<sup>#</sup> Certain commercial equipment and materials are identified in this paper in order to specify adequately the experimental procedure. In no case does such identification imply recommendations by the National Institute of Standards and Technology nor does it imply that the material or equipment identified is necessarily the best available for this purpose.

measurements were performed using a Nicolet NEXUS 670 spectrometer equipped with a MCT/A detector. Final spectra were averaged over 128 scans using a resolution of  $8\text{ cm}^{-1}$ .



*Scheme 1. Acid catalyzed thermally activated deprotection of poly(hydroxystyrene-co-D9-tert-butyl acrylate).*

## RESULTS AND DISCUSSION

Neutron reflectivity measures the buried interface between the acid feeder layer and the deuterated resist copolymer with sub-nm resolution. The normalized reflectivity is plotted versus  $Q_z$  (where  $Q_z$  is the magnitude of the scattering vector normal to the plane of the film) for different exposure doses in Figure 1.  $Q_z$  is a function of the angle of incidence ( $\theta$ ) of the neutron beam with the sample as  $\frac{4\pi}{\lambda} \sin \theta$ . Since neutron reflectivity is sensitive to interfaces<sup>22</sup>, the

dose-effects are clearly measured at the interface between the acid feeder layer and the P(HOSt-co-tBA) copolymer. Changes in the reflectivity curves in Figure 1 result from the photoacid propagation at the model lithographic line edge. A few characteristics of the reflectivity profiles are of note. There is an appreciable change in the bilayer film thickness between the unexposed initial bilayer (black) and exposed or post-exposure baked. This is evident by the increase in Kiessig fringe spacing, corresponding to a decrease in the film thickness. This decrease is attributable to the mass loss upon deprotection, as the t-butyl moiety is converted to the volatile isobutylene. Another characteristic change in the reflectivity profiles is the depth and persistence of the minima. The initial bilayer, which has a sharp, 2 nm interface, shows minima which remain deep to high values of  $Q_z$ . Upon exposure and deprotection, however, the fringes become shallower. Additionally, the curves smooth out at higher  $Q_z$ , indicating broader interfacial widths. The form and extent of deprotection, however, needs to be quantified in order to fully uncover the effect of exposure dose on the reaction front propagation. In order to extract this information from the reflectivity curves we fit the data using established procedures, described elsewhere<sup>20</sup>. The deuteration of the t-butyl protecting group allows a high degree of contrast between the protected and deprotected form of the polymer, allowing sub-nm resolution of the form of the reaction front. The fitting program used was Reffit software developed at the NCNR. Fits to the data are shown as the solid curves in Figure 1. Total extents of deprotection were extracted from fits to the reflectivity data by integrating across the interface and normalizing to the film thickness. This total reaction extent was verified independently using FT-IR spectroscopy.

Fits to the reflectivity data gave a depth profile of our bilayer systems. These data were then converted to deprotection extent as a function of the distance from the model bilayer interface. This allows the direct comparison of the effect of exposure dose on the reaction-diffusion front in our model bilayer. These data are shown in Figure 2 for a PEB at  $90\text{ }^\circ\text{C}$  for 30 s. Two trends of note appear as we observe the propagation of the reaction-diffusion front into the resist copolymer as a function of the concentration of photogenerated acid. One is that the extent of propagation into the film increases with increased exposure dose. At larger doses this extent of propagation is arrested, and even recedes slightly at higher doses. A second trend is that the reaction front appears to proceed at two different length scales; a slow, high deprotection front near the interface and a fast, low deprotection front that propagates into the resist copolymer. In order to quantify extents of propagation for the two fronts a decay length,  $\tau$ , was extracted for the short-ranged front and an interfacial width,  $\sigma$ , was extracted for the long-ranged front.

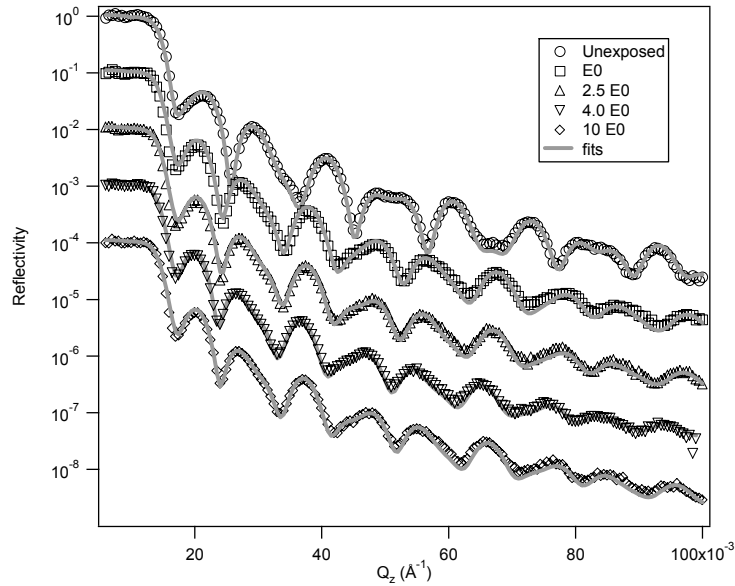


Figure 1. NR profiles for the bilayer samples, obtained as a function of exposure dose, labeled as factors of the dose to clear,  $E_0$ . These samples underwent a PEB at 90 °C for 30 s. The solid lines are least-squared fits to the data. The data are offset by a factor of 1/10 for subsequent doses starting from  $E_0$  to 5.0  $E_0$ .

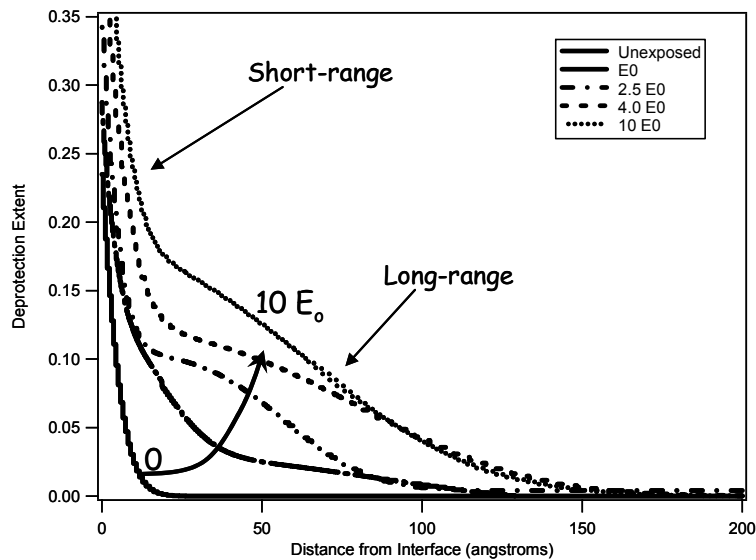


Figure 2. Deprotection profiles at various exposure doses after a PEB at 90 °C for 30 s. Doses are listed as factors of the dose to clear,  $E_0$ .

An example of the curve fitting to the deprotection profiles is shown in Figure 3. The short-ranged front is fit to an exponential of the form  $Y_1 + A_1 \exp(-x / \tau)$ . The long-ranged front is fit to the form  $Y_2 + A_2 \exp\{-[(x - x_2) / \sigma]^2\}$ . The short- and long-ranged diffusion lengths as function of dose, at PEBs of both 90 °C and 130 °C for 30 s, are shown in Figures 4a and b, respectively.

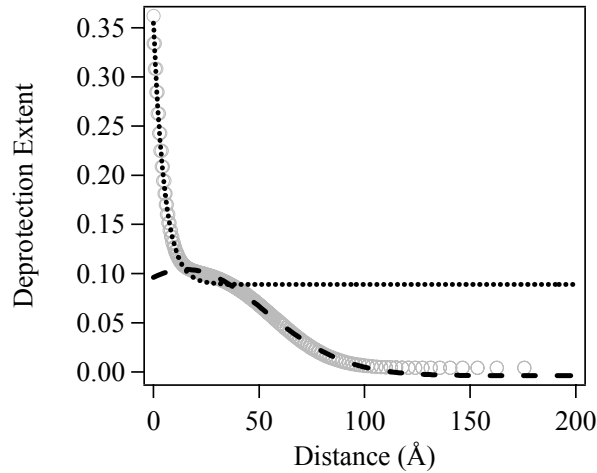


Figure 3. Extraction of the two length scales from the deprotection profile. (---) is used to extract the decay length,  $\tau$ , and (···) is used to extract the interfacial width,  $\sigma$ .

Figure 4a shows that the characteristic length scale for the short-ranged diffusion front proceeds over very short length scales; only as high as 1.2 nm. It should be noted that the deprotection extents over this length scale are very high, as evidenced by the profiles in Figure 3. The deprotection extents reach as high as 0.35 for the 50/50 copolymer. This means that as much as 70 % of the resist copolymer is polar, being either PHOST or PAA. This large polarity shift may be a contributing factor to the large degree to which the reaction front is slowed in this region. It is as if a curtain of acid propagates into the film, initiating high degrees of deprotection and kinetically trapping the acid molecules near the interface. As this is happening, a second reaction front escapes the high deprotection region, initiating lower levels of deprotection over a larger spatial extent.

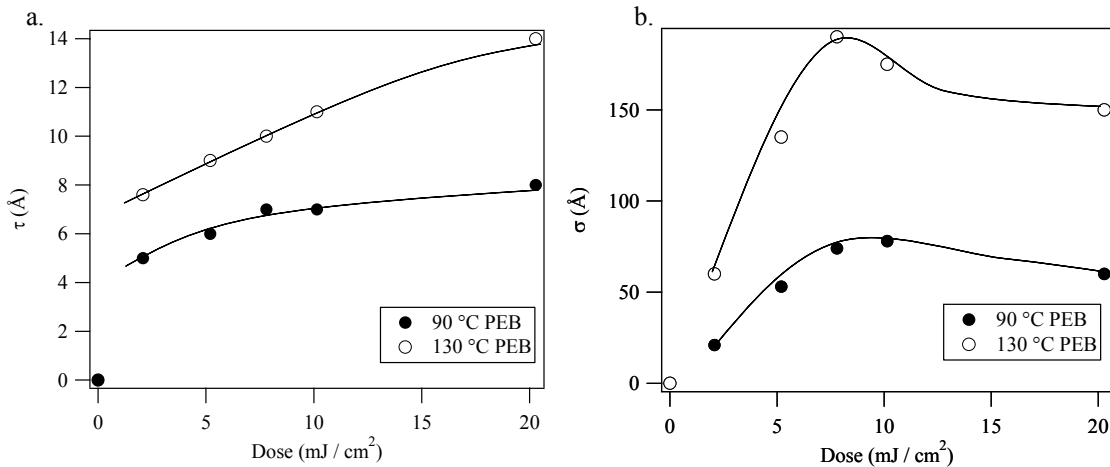


Figure 4. Characteristic reaction-diffusion lengths for (a) the short-ranged diffusion front,  $\tau$ , and (b) the long-ranged diffusion front,  $\sigma$ . Lines are drawn as a guide for the eye.

The long-ranged diffusion, as shown by the diffusion lengths in Figure 4b, occurs over a range of (5 to 15) nm. The length scale and broadness of this deprotection front are problematic to the control of LWR in these systems. Of particular interest is the fact that the length scale over which the long-ranged front acts is dependent on dose. At lower doses, as the amount of photogenerated acid is increased the spatial extent of the reaction front increases. One might expect that, at a constant reaction time and temperature, increasing the concentration of acid would only increase the

degree of deprotection and that the spatial extent of deprotection ( $\sigma$ ) would not change. This is not what we observed, and, instead, the reaction front broadens with an initial increase in dose. Reaction front models that do not consider the change in resist composition upon deprotection would not capture these effects.

Reaction-diffusion coefficients were also extracted for the length scales. These are given in Figures 5a. and b., for the long- and short-ranged fronts, respectively.

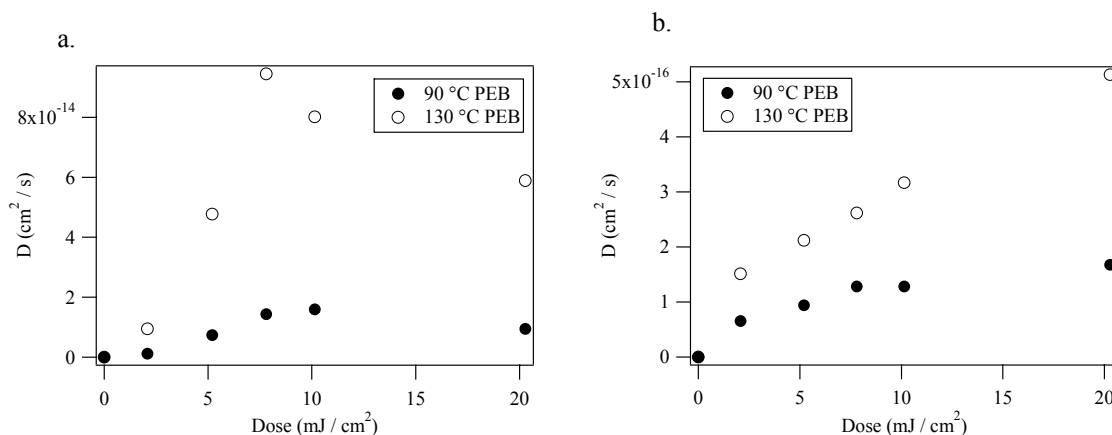


Figure 5. Reaction-diffusion coefficients for (a) the long-ranged diffusion front,  $\sigma$ , and (b) the short-ranged diffusion front,  $\tau$ .

The reaction-diffusion front coefficient ( $D$ ) for the long-ranged front is on the same order of magnitude with the chemical kinetics calculations of Houle *et al.* in which polarity changes resulting from deprotection chemistries were predicted to have a strong influence on the observed reaction-diffusion coefficient<sup>13</sup>. We see that this long-ranged front, also, tends to dominate the overall deprotection observed in the system. Means of determining deprotection extents, such as FT-IR, that integrate across the entire deprotection interface would fail to uncover the slowly propagating front near the exposure line edge. The slowing, and to some extent retraction, of the long-ranged front is possibly due to an increase in the resist polarity near the interface upon deprotection. In terms of LWR it is critical that this fast front be controlled through the use of additives, such as photodegradable bases<sup>15</sup>, in order to increase the prominence of the desirable short-ranged diffusion front. The short-ranged front propagates with a rate two orders of magnitude slower than the fast front, likely due to kinetic trapping of acid molecules in the high-polarity, high deprotection level region near the model exposure line edge.

## CONCLUSIONS

We measured the effect of exposure dose on the reaction-diffusion front in model EUV polymers with a bilayer geometry to serve as an ideal exposure line edge. We observed the progression of deprotection fronts on two different length scales; a slow front that initiates high degrees of deprotection near the interface, and a fast front that propagates into the resist with reaction-diffusion lengths consistent with those reported in the literature. However, the deprotection level and diffusion-length scale are exposure dose (photoacid concentration) dependent. The origin of the fast-diffusion front dependence on dose was hypothesized due to the increase in copolymer composition polarity as the reaction proceeds thereby limiting the spatial-extent. The evolving copolymer composition appears central in future modeling of latent image profiles. This dependence appears even at two different reaction temperatures, but to varying extents. Neutron reflectivity was demonstrated to have sufficient chemical sensitivity and spatial resolution to measure the interfacial structure on sub-nm length scales. This approach can be extended to understand the effects of additives, such as photodegradable bases, on the two length scales.

## ACKNOWLEDGEMENTS

This work was supported by Intel under CRADA 1893 and the NIST Office of Microelectronics Programs. The authors acknowledge Melissa Shell and Christof Krautschik at Intel Corporation for their support and insight, and Jim Sounik and Michael Sheehan at DuPont Electronic Polymers for providing the deuterated polymers used in this study.

### Reference List

1. Ito, H. Chemical Amplification Resists for Microlithography. *Adv Polym Sci* **2005**, *172*, 37-245.
2. Kim, J. H.; Kim, Y. H.; Chon, S. M.; Nagai, T.; Noda, M.; Yamaguchi, Y.; Makita, Y.; Nemoto, H. Influence of acid diffusion length on line edge roughness in KrF photoresists. *Journal of Photopolymer Science and Technology* **2004**, *17* (3), 379-384.
3. Schmid, G. M.; Stewart, M. D.; Singh, V. K.; Willson, C. G. Spatial distribution of reaction products in positive tone chemically amplified resists. *J Vac Sci Techn B* **2002**, *20* (1), 185-190.
4. Stewart, M. D.; Tran, H. V.; Schmid, G. M.; Stachowiak, T. B.; Becker, D. J.; Willson, C. G. Acid catalyst mobility in resist resins. *Journal of Vacuum Science & Technology B* **2002**, *20* (6), 2946-2952.
5. Wallraff, G. M.; Hinsberg, W. D. Lithographic Imaging Techniques for the Formation of Nanoscopic Features. *Chem. Rev.* **1999**, *99*, 1802-1821.
6. Jones, R. L.; Prabhu, V. M.; Goldfarb, D. L.; Lin, E. K.; Soles, C. L.; Lenhart, J. L.; Wu, W. L.; Angelopoulos, M. Correlation of the reaction front with roughness in chemically amplified photoresists. 874 ed.; American Chemical Society: Washington D.C., 2004; pp 86-97.
7. Nakamura, J.; Ban, H.; Tanaka, A. Influence of Acid Diffusion on the Lithographic Performance of Chemically Amplified Resists. *Japanese Journal of Applied Physics Part 1-Regular Papers Short Notes & Review Papers* **1992**, *31*, 4294-4300.
8. Pawloski, A.; Acheta, A.; Lalovic, I.; La Fontaine, B.; Levinson, H. Characterization of line-edge roughness in photoresist using an image fading technique. *Proceedings of the SPIE - The International Society for Optical Engineering* **2004**, vol.5376, no.1, 414-425.
9. Postnikov, S. V.; Stewart, M. D.; Tran, H. V.; Nierode, M. A.; Medeiros, D. R.; Cao, T.; Byers, J.; Webber, S. E.; Willson, C. G. Study of resolution limits due to intrinsic bias in chemically amplified photoresists. *Journal of Vacuum Science & Technology B* **1999**, *17* (6), 3335-3338.
10. Wallraff, G.; Hutchinson, J.; Hinsberg, W. D.; Houle, F. A.; Seidel, P.; Johnson, R.; Oldham, W. Thermal and acid-catalyzed deprotection kinetics in candidate deep ultraviolet resist materials. *Journal of Vacuum Science & Technology B* **1994**, *12* (6), 3857-3862.
11. Pawloski, A. R.; Nealey, P. F. Effect of photoacid generator concentration on sensitivity, photoacid generation, and deprotection of chemically amplified resists. *Journal of Vacuum Science & Technology B* **2002**, *20* (6), 2413-2420.
12. Goldfarb, D. L.; Angelopoulos, M.; Lin, E. K.; Jones, R. L.; Soles, C. L.; Lenhart, J. L.; Wu, W. L. Confinement effects on the spatial extent of the reaction front in ultrathin chemically amplified photoresists. *Journal of Vacuum Science & Technology B* **2001**, *19* (6), 2699-2704.

13. Hinsberg, W. D.; Houle, F. A.; Sanchez, M. I.; Wallraff, G. M. Chemical and physical aspects of the post-exposure baking process used for positive-tone chemically amplified resists. *Ibm Journal of Research and Development* **2001**, *45* (5), 667-682.
14. Schlegel, L.; Ueno, T.; Hayashi, N.; Iwayanagi, T. Determination of acid diffusion in chemical amplification positive deep ultraviolet resists. *J Vac Sci Techn B* **1991**, *9* (2), 278-289.
15. Houle, F. A.; Hinsberg, W. D.; Morrison, M.; Sanchez, M. I.; Wallraff, G.; Larson, C.; Hoffnagle, J. Determination of coupled acid catalysis-diffusion processes in a positive-tone chemically amplified photoresist. *J Vac Sci Techn B* **2000**, *18* (4), 1874-1885.
16. Lin, E. K.; Soles, C. L.; Goldfarb, D. L.; Trinque, B. C.; Burns, S. D.; Jones, R. L.; Lenhart, J. L.; Angelopoulos, M.; Willson, C. G.; Satija, S. K.; Wu, W. L. Direct Measurement of the Reaction Front in Chemically Amplified Photoresists. *Science* **2002**, *297*, 372-375.
17. Zuniga, M.; Wallraff, G. M.; Neureuther, A. R. Reaction diffusion kinetics in deep-UV positive-tone resist systems. *Proceedings of the SPIE - The International Society for Optical Engineering* **1995**, *2438*, 113-124.
18. Nagahara, S.; Yuan, L.; Poppe, W. J.; Neureuther, A.; Kono, Y.; Sekiguchi, A.; Fujiwara, K.; Watanabe, T.; Taira, K.; Kusumoto, S.; Nkano, T.; Shimokawa, T. Understanding quencher mechanisms by considering photoacid-dissociation equilibrium in chemically-amplified resists. *Proceedings of SPIE* **2005**, *5753*.
19. Houle, F. A.; Hinsberg, W. D.; Sanchez, M. I. Acid-base reactions in a positive tone chemically amplified photoresist and their effect on imaging. *Journal of Vacuum Science & Technology B* **2004**, *22* (2), 747-757.
20. Lin, E. K.; Soles, C. L.; Goldfarb, D. L.; Trinque, B. C.; Burns, S. D.; Jones, R. L.; Lenhart, J. L.; Angelopoulos, M.; Willson, C. G.; Satija, S. K.; Wu, W. L. Direct measurement of the reaction front in chemically amplified photoresists. *Science* **2002**, *297* (5580), 372-375.
21. Press, W. *Numerical recipes : the art of scientific computing*; Cambridge University Press: Cambridge, 1986.
22. Russell, T. P. X-ray and neutron reflectivity for the investigation of polymers. *Mater. Sci. Rep.* **1990**, *5*, 171-271.